Journal of Power Sources 263 (2014) 209–216

Contents lists available at ScienceDirect

Journal of Power Sources

journal homepage: www.elsevier.com/locate/jpowsour

Mixed ion/electron-conductive protective soft nanomatter-based conformal surface modification of lithium-ion battery cathode materials

Jang-Hoon Park [a], Ju-Myung Kim [a], Chang Kee Lee [b], Sang-Young Lee [a,*]

[a] Interdisciplinary School of Green Energy, Ulsan National Institute of Science and Technology (UNIST), Ulsan 689-798, Republic of Korea
[b] Korea Packaging Center, Korea Institute of Industrial Technology, Bucheon, Gyeonggi-do 421-742, Republic of Korea

HIGHLIGHTS

- Conformal surface modification of lithium battery cathode materials is presented.
- Mixed ion (PI)/electron (C)-conductive soft nanomatter is used as a coating layer.
- PI/C nanolayer is synthesized on $LiCoO_2$ surface via one-pot thermal treatment.
- Multifunctional coating enables electronic facilitation and side reaction suppression.
- Synergistic coating effect improves high-voltage performance and thermal stability.

GRAPHICAL ABSTRACT

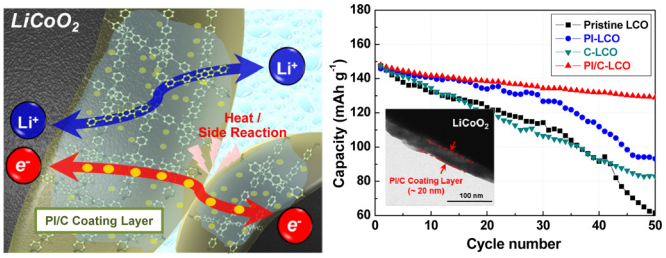

ARTICLE INFO

Article history:
Received 27 February 2014
Received in revised form
4 April 2014
Accepted 7 April 2014
Available online 24 April 2014

Keywords:
Lithium-ion batteries
Interfacial phenomena
Cathode materials
Liquid electrolytes
Conformal surface modification
Mixed ion/electron-conductive soft nanomatter

ABSTRACT

Understanding and control of interfacial phenomena between electrode material and liquid electrolytes are of major scientific importance for boosting development of high-performance lithium ion batteries with reliable electrochemical/safety attributes. Here, as an innovative surface engineering approach to address the interfacial issues, a new concept of mixed ion/electron-conductive soft nanomatter-based conformal surface modification of the cathode material is presented. The soft nanomatter is comprised of an electron conductive carbonaceous (C) substance embedded in an ion conductive polyimide (PI) nanothin compliant film. In addition to its structural uniqueness, the newly proposed surface modification benefits from a simple fabrication process. The PI/carbon soft nanomatter is directly synthesized on $LiCoO_2$ surface via one-pot thermal treatment of polyamic acid (=PI precursor) and sucrose (=carbon source) mixture, where the $LiCoO_2$ powders are chosen as a model system to explore the feasibility of this surface engineering strategy. The resulting PI/carbon coating layer facilitates electronic conduction and also suppresses unwanted side reactions arising from the cathode material-liquid electrolyte interface. These synergistic coating effects of the multifunctional PI/carbon soft nanomatter significantly improve high-voltage cell performance and also mitigate interfacial exothermic reaction between cathode material and liquid electrolyte.

* Corresponding author. Tel.: +82 52 217 2948; fax: +82 52 217 2019.
E-mail address: syleek@unist.ac.kr (S.-Y. Lee).

http://dx.doi.org/10.1016/j.jpowsour.2014.04.028
0378-7753/

1. Introduction

High energy density lithium-ion batteries with well-fledged electrochemical characteristics have been aggressively pursued as promising power sources for rapidly growing industries such as smart mobile electronics, (hybrid) electric vehicles, and grid energy storage systems [1–3]. A major challenge to the development of these advanced batteries, in terms of materials chemistry and engineering, arises from an interfacial instability between the electrode material and liquid electrolyte, in addition to structural/chemical deficiencies of major cell components. Meanwhile, as a simple and effective way to increase the energy density (i.e., energy [J] = coulombic capacity [C] × voltage [V]) of cells, a high-voltage cell strategy has garnered considerable attention [4,5]. Unfortunately, under such high-voltage operating conditions, the unwanted interfacial side reactions between delithiated cathode materials and carbonate-based liquid electrolytes become more serious, thus posing a critical threat to electrochemical performance (in particular, cycling performance) and thermal stability of the cells. Hence, in-depth understanding and control of the interfacial phenomena between the cathode materials and liquid electrolytes, along with research efforts on the synthesis of new electrochemically active materials, are critically needed as essential prerequisites to further development.

One popular approach to resolve the interfacial problem is surface modification of the cathode materials using inorganic materials [6–9] such as Al_2O_3, ZrO_2, $AlPO_4$, and AlF_3. Although the inorganic coatings have been found to suppress the interfacial side reactions, the inorganic substances are discontinuously deposited on cathode materials and also remain as an ionically/electronically resistive layer. As a consequence, Faradaic reaction kinetics at the cathode material-liquid electrolyte interface could be impaired, overshadowing the advantageous effects of the inorganic coatings.

Our group recently reported a new surface modification strategy based on an ion-conductive polyimide (PI) thin layer [10–12]. The PI coating layer exhibited continuous surface coverage, and facile ion transport through the electrolyte-swollen PI nanothin film. Despite these advantageous effects, the PI coating layers were electronically inert, which remains a big obstacle to attaining a satisfactory level of cell performance.

In the present study, as an innovative surface engineering approach to address the interfacial issues between cathode materials and liquid electrolytes, we demonstrate a new concept of mixed ion/electron-conductive soft nanomatter-mediated conformal surface modification, which is different from the abovementioned inorganic or PI coatings. The unique soft nanomatter is comprised of an electron conductive carbonaceous (C) substance embedded in an ion conductive polyimide (PI) nanothin compliant film. The research motivation for ion/electron-conductive coating layers came from a previous suggestion by Zhou and his co-workers [13]. They reported the potential advantages of "hybrid coating" (i.e., an ion/electron-conductive coating layer) at the electrode material-liquid electrolyte interface; however, very little experimental proof-of-concept has been reported [14].

A salient contribution of the PI/C soft nanomatter-based surface modification presented here is its multifunctional coating effect, which alleviates side reactions arising from the cathode material–liquid electrolyte interface (due to the beneficial influence of PI) and also facilitates electronic conduction (a positive contribution of C). Importantly, the newly proposed surface modification benefits from a simple fabrication process. The PI/C coating layer is directly synthesized on the surface of the cathode material via one-pot thermal treatment of polyamic acid (=PI precursor) and sucrose [15–17] (=carbon source) mixture. Here, $LiCoO_2$ (LCO) powders are chosen as a model system. Based on a structural/physicochemical characterization of the PI/C soft nanomatter-coated LCO (hereinafter, referred to as "PI/C-LCO"), the effects of the PI/C-LCO on cell performance (with a focus on harsh operating conditions of high voltage and fast current density) and also exothermic reaction with liquid electrolyte are investigated. The unusual multifunctionality of the PI/C soft nanomatter at the LCO-liquid electrolyte interface is discussed in terms of a mixed ion/electron-conductive protective conformal coating layer.

2. Experimental procedures

2.1. Synthesis of PI/C soft nanomatter-coated LCO powders

A pyromellitic dianhydride (PMDA)/oxydianiline (ODA) (=1.00/1.01, molar ratio)-based polyamic acid solution was synthesized using dimethyl acetamide (DMAc) as a solvent under nitrogen atmosphere. The detailed synthesis procedure of the polyamic acid was described in previous publications [18,19]. The polyamic acid solution was then mixed with sucrose (Mw = 342 g mol^{-1}, Aldrich). The composition ratio of polyamic acid/sucrose was fixed at 50/50 w/w. After preparing the polyamic acid/sucrose solution, LCO powders (average particle size = 5 μm, Umicore) were added into the mixture solution and then subjected to ultrasonication to achieve uniform dispersion. After filtering and vacuum-drying, the polyamic acid/sucrose mixture-deposited LCO powders were obtained and then subjected to one-pot thermal treatment. The one-pot reaction enabled the carbonization of sucrose and thermal-imidization of the polyamic acid at the same time, leading to the direct formation of PI/C soft nanomatter on the LCO particle surfaces. The thermal reaction condition was set as 60 °C for 30 min → 120 °C for 30 min → 200 °C for 60 min → 300 °C for 60 min → 400 °C for 10 min under nitrogen atmosphere. A schematic representation depicting the synthesis procedure of PI/C-LCO, along with the chemical structures of polyamic acid, sucrose, and the resulting PI/C, is shown in Scheme 1.

2.2. Characterization of PI/C soft nanomatter-coated LCO powders and their effect on electrochemical performance/thermal stability of high-voltage cells

The surface morphology of PI/C-LCO was characterized using field emission scanning electron microscopy (FE-SEM, Hitachi) equipped with an energy-dispersive spectrometer (EDS) and transmission electron microscopy (TEM, JEOL). The thermal stability of PI and sucrose was characterized with a thermogravimetric analyzer (TGA, TA Instruments). The carbonaceous structure of PI/C-LCO was elucidated using a Raman monochromator (ARAMIS, Horiba Jobin). The phase-separated microstructure of PI/C coating layer was elucidated by analyzing FT-IR characteristic peaks (FT-IR spectrometer, FT-3000, Excalibur) and EDS images. The LCO cathode was fabricated by coating NMP-based slurry with a mixture of 95 wt.% of LCO, 3 wt.% of polyvinylidene fluoride binder, and 2 wt.% of carbon black additive on an aluminum current collector. A unit cell (2032-type coin) was assembled by sandwiching a PE separator (thickness = 20 μm, Tonen) between the PI/C-LCO cathode (thickness = 50 μm) and natural graphite anode (natural graphite/PVdF/carbon black = 90/8/2 w/w/w, thickness = 30 μm). The areal mass loadings of the cathode and anode were 16.1 and 8.5 mg cm^{-2}, respectively. Then, liquid electrolyte of 1 M $LiPF_6$ in ethylene carbonate (EC)/ethyl methyl carbonate (EMC) = 1/2 v/v (Soulbrain) was injected into the coin cell. The discharge capacities and rate capability of the cells were evaluated by varying discharge current densities (i.e., discharge C-rates) from 0.2 (=0.52 mA cm^{-2}) to 2.0 C at a constant charge current density of 0.2 C. The cells were cycled at constant charge/discharge current densities of 1.0 C/1.0 C under a

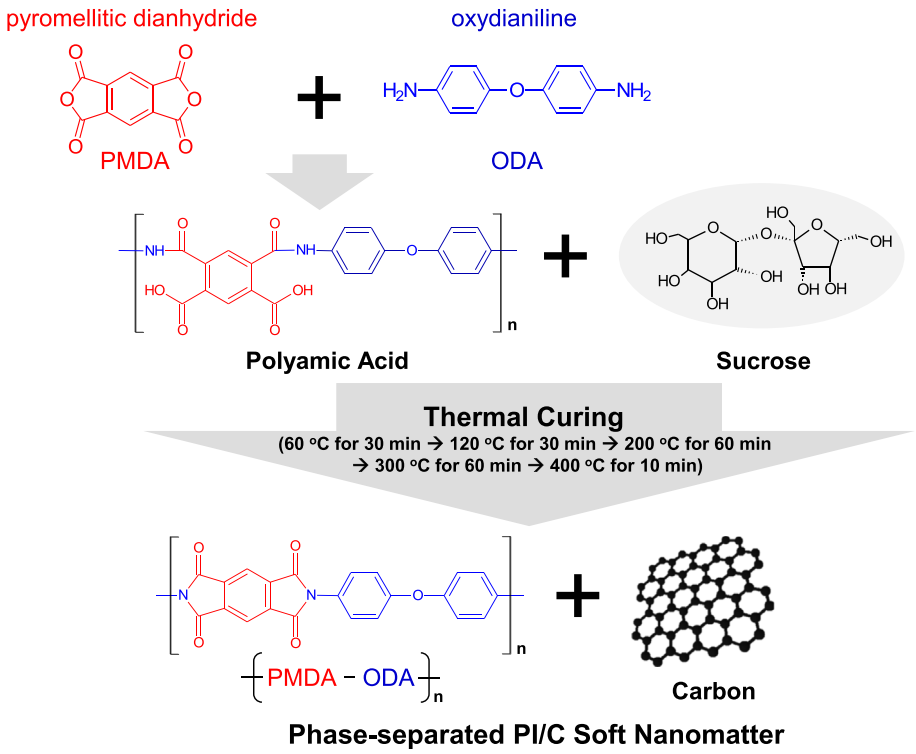

Scheme 1. Chemical structures of PMDA/ODA polyamic acid, sucrose, and PI/C soft nanomatter. The one-pot thermal treatment condition of polyamic acid/sucrose mixture for direct synthesis of a PI/C coating layer on $LiCoO_2$ surface is also depicted.

voltage range of 3.0 – 4.4 V. The AC impedance (frequency range = 10^{-3} to 10^{6} Hz at an amplitude of 10 mV) and cyclic voltammetry (scan rate = 0.1 mV s^{-1} under 2.5 – 4.4 V) of the cells were obtained using a potentiostat/galvanostat equipped with an impedance analyzer (VSP classic, Bio-Logic). The interfacial exothermic reaction between the charged LCO and liquid electrolyte was investigated with differential scanning calorimetry (DSC, TA Instruments) measurements, where the cells were charged to 4.4 V at a current density of 0.1 C and then disassembled in a dry room to remove the charged cathode. The DSC measurements were performed under temperature ranging from room temperature to 350 °C at a heating rate of 10 °C min^{-1}.

3. Results and discussions

A noteworthy benefit of PI/C-LCO powders, in terms of their synthesis procedure, is the one-pot thermal treatment of polyamic acid (=PI precursor) and sucrose (=carbon source) mixture on the LCO surface. The thermal reaction condition was determined by analyzing the TGA results of the sucrose and PI. It is known that sucrose turns into a kind of carbonaceous materials after thermal combustion (i.e., calcination) above a temperature of 400 °C [17]. The sucrose used in this study also showed similar thermal behavior (Fig. S1a, Supporting information). Meanwhile, the polyimide was found to be thermally stable up to 500 °C (Fig. S1b, Supporting information). From these TGA results of sucrose and PI, the one-pot thermal reaction condition was set not to exceed a temperature of 500 °C (more details are described in the Experimental section). Any further increase of thermal treatment temperature and time, which may be effective for calcination of sucrose, is not recommended because unwanted thermal decomposition of PI may occur. Optimization of the one-pot reaction condition, which undoubtedly contributes to maximizing the advantageous effects of the PI/C coating layer, will be conducted in our future studies.

The structural uniqueness of PI/C-LCO was characterized, with a focus on the PI/C coating layer. In comparison to the pristine LCO, which shows the smooth planes and well-defined edges (inset image of Fig. 1a), a different surface morphology was observed for the PI/C-LCO (Fig. 1a). In addition to the PI thin film, the sucrose-derived carbonaceous substances are observed on the LCO surface, demonstrating the formation of a PI/C-based conformal coating layer. This unusual surface morphology of the PI/C-LCO was further elucidated by TEM analysis. Fig. 1b shows that a PI/C nanothin film having a thickness of ~20 nm has been deposited on the LCO surface, although a perfectly uniform coating layer is not yet achieved. Meanwhile, as reference samples, surface morphology of the PI-coated LCO (denoted as "PI-LCO") and carbon-coated LCO ("C-LCO") was also investigated (Fig. S2, Supporting information). The PI-LCO evidently shows the formation of nanometer-thick PI coating layers (thickness ~ 20 nm), while sucrose-derived carbonaceous particles are randomly distributed on the C-LCO surface.

The in-depth analysis of Raman spectra delivered valuable information on the structure of PI/C-LCO. Two characteristic Raman bands assigned to the layered-hexagonal phase of LCO (Fig. 1c) are observed at around 495 (corresponding to Raman active mode E_g) and 601 cm^{-1} (Raman active mode A_{1g}) [20]. It is worth noting that the corresponding peak intensities diminish with the introduction of PI/C coating layers, which may confirm that the LCO powders have been covered with the PI/C coating layers. In addition, the PI/C-LCO (Fig. 1d) presents the two broad bands assigned to carbonaceous materials [21,22] appearing at 1346 cm^{-1} (D-band for amorphous form) and 1596 cm^{-1} (G-band for graphitic form). Although the exact comparison of the two bands is difficult to determine from the Raman spectra, the relatively stronger intensity of the D-band may indicate that a large portion of the carbonaceous

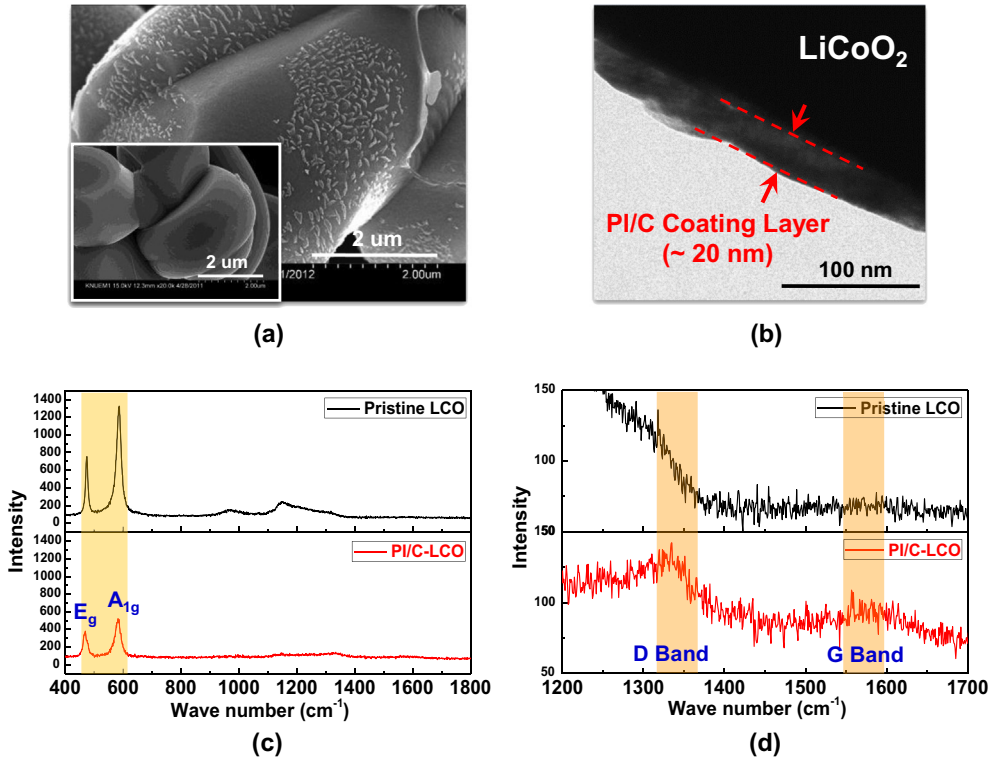

Fig. 1. Structural characterization of PI/C-LCO: (a) FE-SEM photograph (inset is an image of pristine LCO); (b) TEM photograph; (c) Raman spectra under a wave number range of 400 − 1800 cm^{-1}. (d) Raman spectra under a wave number range of 1200 − 1700 cm^{-1}.

substances in the PI/C coating layer are in an amorphous phase. It was previously reported that a calcination temperature below 1000 °C tends to preferentially yield amorphous carbon [23–25].

The XRD patterns show that no significant difference can be detected between the pristine and PI/C-LCO (Fig. S3, Supporting information), both of which have the typical layered structure of hexagonal α-$NaFeO_2$ type with $R\bar{3}m$ space group [26]. The lattice parameters of the LCO powders were calculated from the Rietveld refinement of the XRD results. The estimated lattice parameters are $a = 2.82$ Å/$c = 14.03$ Å for pristine LCO and $a = 2.82$ Å/$c = 14.04$ Å for PI/C-LCO, respectively. This XRD result indicates that the introduction of the PI/C coating layer does not disrupt the layered crystalline structure of bulk LCO.

To gain a more comprehensive understanding of the microstructure of the PI/C coating layer, its phase separation behavior was investigated. Unfortunately, direct characterization of the PI/C-LCO did not provide meaningful results, possibly due to the extremely small amount of coating layers. Instead, a free-standing PI/C film (thickness ~ 50 μm) was prepared as a model system using the same fabrication procedure employed for the PI/C coating layers. The FT-IR peaks (Fig. 2a) show no appreciable difference between the PI and PI/C film, indicating that the polyamic acid was successfully cured to form PI in the PI/C film and also that the resulting PI may not be miscible with carbonaceous materials. The microstructure of the PI/C film was further elucidated by analyzing the EDS image (Fig. 2b). It is apparent that a carbon-rich phase (assigned to the black region, atomic composition ratio of C/O = 82/18) and carbon-poor phase (gray region, atomic composition ratio of C/O = 52/48) co-exist in the PI/C. In addition to the FT-IR result, this EDS image is further evidence that the PI and carbonaceous materials are heterogeneously mixed, leading to the formation of phase-separated structure. Hence, it can be reasonably expected that the advantageous feature of each component (i.e., PI and carbonaceous materials) in the PI/C coating layer will be preserved, thereby enabling the realization of a synergistic coating effect for improving the electrochemical performance of cells assembled with PI/C-LCO.

Based on the abovementioned structural characterization of the PI/C coating layer, the effects of PI/C-LCO on high-voltage (here, 4.4 V) cell performance were investigated. Firstly, the discharge capacities and discharge rate capability of the cells were evaluated, wherein discharge current densities were varied from 0.2 (=0.52 mA cm^{-2}) to 2.0 C at a constant charge current density of 0.2 C under the operating voltage range of 3.0 − 4.4 V. All LCO samples examined herein show a typical voltage plateau and a discharge capacity of approximately 160 mAh g^{-1} at a discharge current density of 0.2 C (Fig. 3a). As the discharge current density was increased to 2.0 C, the influence of cell polarization [27,28] in the discharge profiles was found to be more significant (Fig. S4, Supporting information). Among the LCO samples, the PI-LCO presents the lowest discharge rate capability, indicating that the electronically-inert PI coating layer (despite allowing ionic transport) causes an undesirable rise in cell polarization. On the other hand, the C-LCO and also the PI/C-LCO show the excellent discharge rate capability, as compared to the pristine LCO (Fig. 3b). It is believed that surface modification of electrode materials with carbonaceous materials could establish extra electron-conductive pathways among the electrode particles and also with current collectors [15–17]. For this reason, the newly-formed electroconductive carbonaceous materials in the PI/C-LCO could exert a beneficial influence on the discharge rate capability.

The noticeable difference in the discharge rate capability between the PI-LCO and PI/C-LCO was verified by comparing their electronic conductivity and also the initial (i.e., after formation) AC impedance of the cells. The electronic conductivity of the LCO samples was estimated using 4-point probe measurement. For this

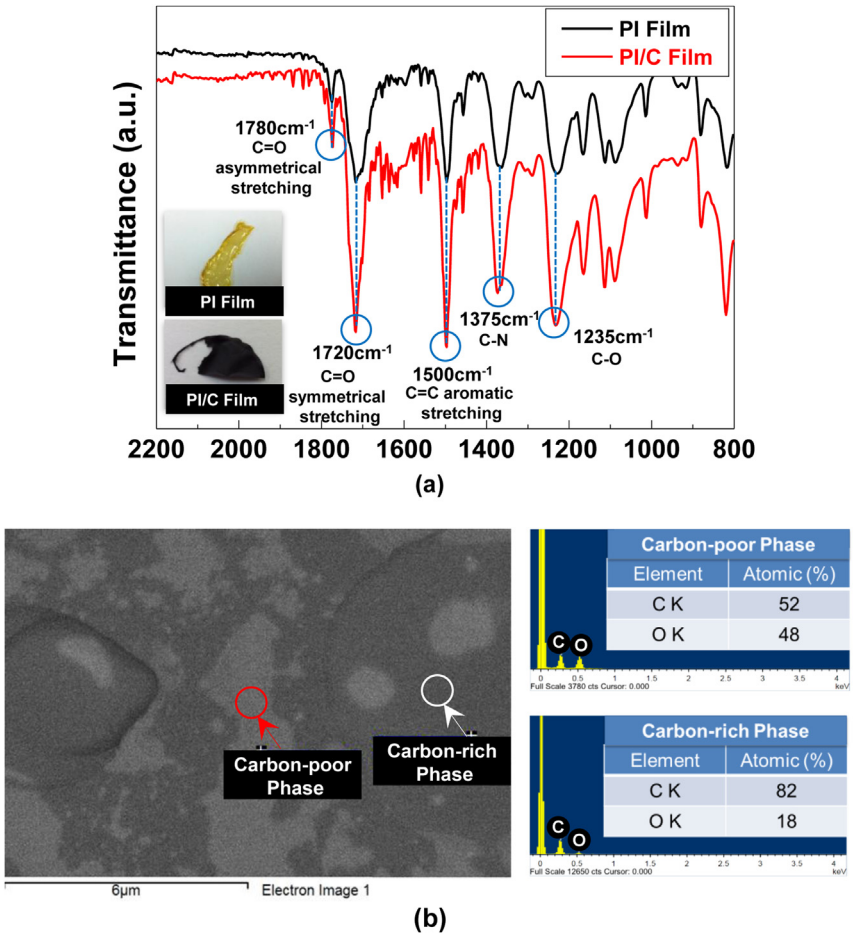

Fig. 2. Microstructural analysis of free-standing PI/C film: (a) comparison of FT-IR spectra between PI film and PI/C film; (b) EDS image showing phase-separated structure of PI/C film (the black region and gray region represent carbon-rich phase and carbon-poor phase, respectively).

characterization, LCO cathode discs solely comprised of LCO powders without conductive additives such as carbon black powders were fabricated. Here, to facilitate the preparation of free-standing LCO cathode discs, a very small amount (=1.5 wt.%) of styrene butadiene rubber (SBR) binder was added. Unfortunately, the presence of the SBR binder may cause an unwanted rise in the electronic resistance of the LCO cathode discs. Therefore, the electronic resistivity data obtained from this measurement is restricted to a relative comparison between the samples, instead of providing absolute values. In accordance with our expectation, the PI/C-LCO showed higher electronic conductivity ($\sim 6.0 \times 10^{-7}$ S cm^{-1}) than the PI-LCO ($\sim 1.1 \times 10^{-7}$ S cm^{-1}). In addition, the comparison of initial cell impedance (Fig. S5, Supporting information) exhibits that the PI/C-LCO had lower cell impedance ($Z_{Re} \sim 19\ \Omega$) than the PI-LCO ($Z_{Re} \sim 32\ \Omega$). These results demonstrate that the incorporation of an electroconductive carbonaceous substance is an effective way to overcome the critical drawback (associated with poor electronic conduction) of the PI coating layer.

The effect of PI/C-LCO on the high-voltage cycling performance (i.e., capacity retention as a function of cycle number) of cells was investigated, where the cells were cycled between 3.0 and 4.4 V at a fixed charge/discharge current density (=1.0 C/1.0 C). Fig. 3c shows that the charge/discharge capacities of the pristine LCO sharply decrease with cycling, resulting in a very low discharge capacity of 63 mAh g^{-1} after the 50th cycle. By comparison, for the PI/C-LCO, the charge/discharge capacities are not severely impaired during charge/discharge cycling, although the number of charge/discharge cycles examined herein is not so large. This improved capacity retention of PI/C-LCO can be further explained by the mitigation in growth of cell polarization (shown from the charge–discharge profile) after the 50th cycle.

The cycling performance of the various LCO samples is summarized in Fig. 3d. Whereas the discharge capacity of the pristine LCO continues to decline with cycling, the capacity fading of the PI-LCO and PI/C-LCO is substantially retarded. Meanwhile, the improvement in the capacity retention of the C-LCO is relatively small compared to the PI-LCO and PI/C-LCO cases. After the 50th cycle, the capacity retentions are respectively 42 % for the pristine LCO, 56 % for the C-LCO, 64 % for the PI-LCO, and 87 % for the PI/C-LCO. Our previous studies [10–12] reported that the PI coating layers protect the LCO surface from direct attack by liquid electrolyte, which thus alleviates unwanted interfacial side reactions between the cathode material and liquid electrolyte. Here, it should be noted that, in addition to the abovementioned beneficial functions of the PI coating layers, the electroconductive carbonaceous substance in the PI/C coating layer synergistically improves the high-voltage cycling performance. This unique multifunctionality of the PI/C coating layer, as a mixed ion/electron-conductive protective conformal soft nanomatter film, is conceptually illustrated in Fig. 4.

In an endeavor to better understand the superior cycling performance of PI/C-LCO, the variation in AC impedance spectra of 4.4 V-charged cells after the 1st and 50th cycle (charge/discharge current density = 1.0 C/1.0 C) were analyzed. Fig. 5a shows that the cell impedance of pristine LCO significantly increases after the 50th

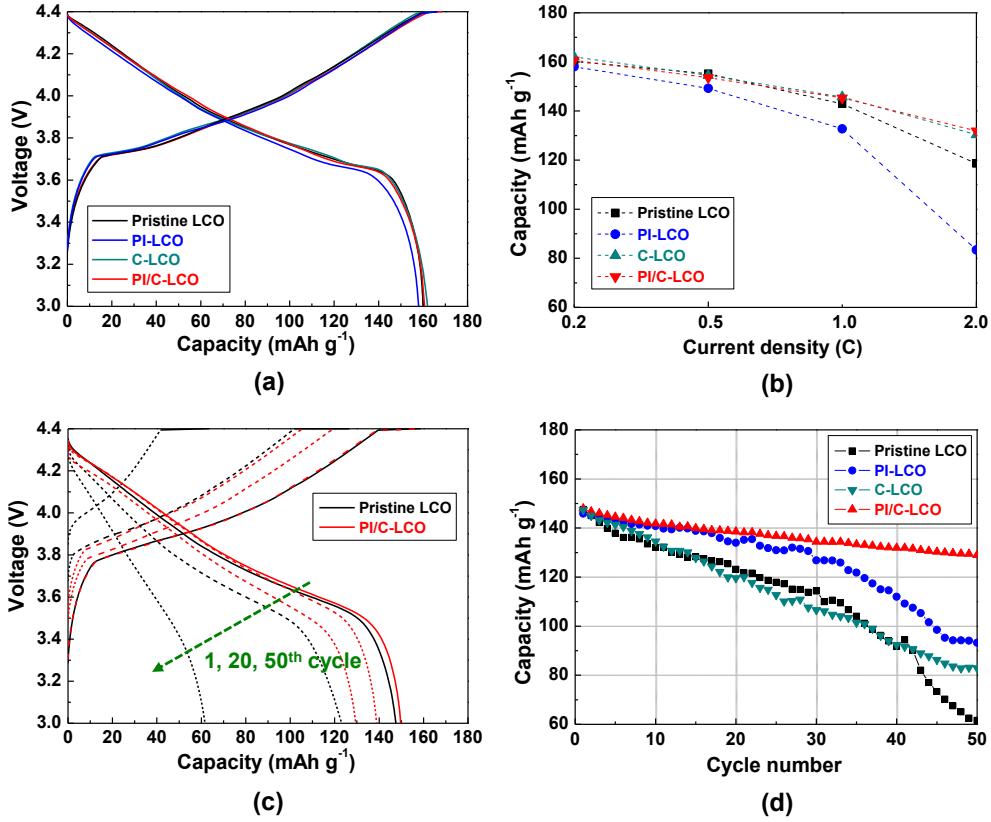

Fig. 3. High-voltage cell performance under a voltage range of 3.0 – 4.4 V: (a) charge/discharge profiles of pristine LCO, C-LCO, PI-LCO, and PI/C-LCO (charge/discharge current density = 0.2 C/0.2 C); (b) comparison of discharge rate capability between pristine LCO, C-LCO, PI-LCO, and PI/C-LCO, where discharge current densities are varied from 0.2 to 2.0 C; (c) variation in charge/discharge profiles of pristine LCO and PI/C-LCO as a function of cycle number (charge/discharge current density = 1.0 C/1.0 C); (d) comparison of cycling performance between pristine LCO, C-LCO, PI-LCO, and PI/C-LCO.

cycle (Z_{Re} (50th cycle) – Z_{Re} (1st cycle) = ΔZ_{Re} ~ 2300 Ω). Considering a possible equivalent circuit (the inset of Fig. 5b) [17,29,30] for the AC impedance spectra of cells, such a large increase in cell impedance reveals that the capacity fading of pristine LCO may be attributed to the formation of undesired resistive layers that impede charge transfer across the LCO surface during cycling. In comparison, the growth of cell impedance is suppressed for the PI-LCO (ΔZ_{Re} ~ 800 Ω) (Fig. S6a, Supporting information), which reveals the positive influence of the PI coating layer on preventing direct exposure of delithiated LCO to liquid electrolyte during the high-voltage cycling. Meanwhile, for the C-LCO, the growth of cell impedance is not sufficiently retarded (Fig. S6b, Supporting information), which is consistent with the result of cycling performance. By comparison, a remarkable improvement in cell impedance was observed for the PI/C-LCO (Fig. 5b). The growth of cell impedance after the 50th cycle is considerably suppressed (ΔZ_{Re} ~ 40 Ω).

These AC impedance analysis results verify the unusual synergistic effect (i.e., combination of ion-conductive protective PI nanothin film with electron-conductive carbonaceous substance) of PI/C coating layers on the improvement of cycling performance. In order to provide more comprehensive information on the variation of AC impedance with cycling, a more detailed analysis of the impedance spectra was undertaken on the basis of the proposed equivalent circuit. The calculated impedance parameters are summarized in Table S1 (Supporting information), where R_e is the electrolyte resistance, R_s is the surface resistance and R_{ct} is the charge transfer resistance [17,30].

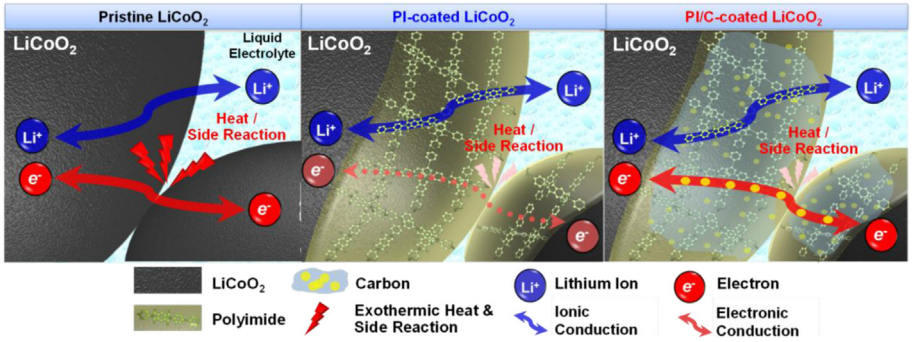

Fig. 4. A conceptual representation illustrating the synergistic coating effects of PI/C soft nanomatter (as a mixed ion/electron-conductive protective conformal coating layer) for controlling interfacial phenomena between $LiCoO_2$ and liquid electrolyte.

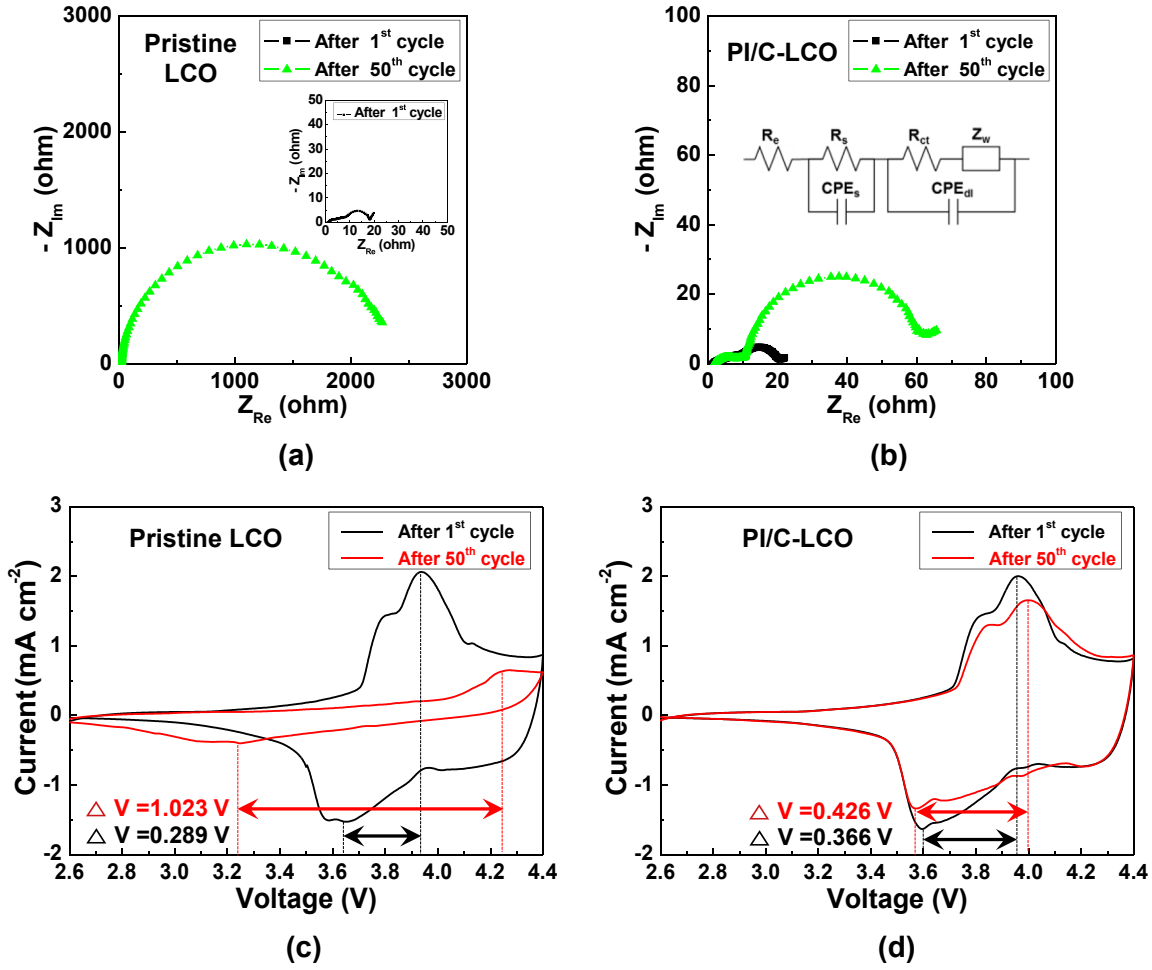

Fig. 5. Electrochemical analysis of cells during charge/discharge cycling ($1^{st} \rightarrow 50^{th}$ cycle). Variation in AC impedance spectra (under a frequency range of $10^{-3} - 10^{6}$ Hz) of: (a) pristine LCO, wherein the inset shows AC impedance spectra after 1^{st} cycle; (b) PI/C-LCO, wherein the inset depicts the proposed equivalent circuit comprising resistors (R), constant phase elements (CPE) and Warburg element (Z_W). Variation in cyclic voltammograms (at a scan rate of 0.1 mV s^{-1}) of: (a) pristine LCO; (d) PI/C-LCO.

Additional evidence of the advantageous effect of PI/C-LCO on high-voltage cycling performance was obtained by estimating the variation in electrode polarization during cycling using cyclic voltammetry (CV). For the pristine LCO (Fig. 5c), the potential difference (=ΔV) between the anodic and cathodic peak increases from 0.289 V (after the 1^{st} cycle) to 1.023 V (after the 50^{th} cycle). Meanwhile, the growth of ΔV with cycling is suppressed for the PI/C-LCO (Fig. 5d, $\Delta V = 0.366$ V (after the 1^{st} cycle) $\rightarrow$ 0.426 V (after the 50^{th} cycle)). The CV result exhibits that, during high-voltage cycling, the Faradaic reaction involving (de)intercalation of lithium ions may be less impaired in the PI/C-LCO. This is indirect evidence that the PI/C coating layer could be effective in preventing the formation of unwanted resistive layers on LCO surfaces.

Finally, the effect of the PI/C coating layer on the thermal stability of high voltage (4.4 V)-charged LCO was investigated using DSC measurement. Fig. 6 shows that the pristine LCO yields a large exothermic heat ($\Delta H = 706$ J g^{-1}) and low exothermic peak temperatures ($T_{peak} = 218, 243$ °C) due to an undesirable interfacial side reaction with the liquid electrolyte [6,9]. On the other hand, for the PI/C-LCO, the exothermic heat is considerably reduced and the exothermic peaks also shift to higher temperatures ($\Delta H = 403$ J g^{-1}, $T_{peak} = 219, 251$ °C), which are comparable to the DSC results of the PI-LCO ($\Delta H = 434$ J g^{-1}, $T_{peak} = 219, 250$ °C). No appreciable difference in the DSC profiles was observed between the pristine LCO and C-LCO, indicating that the carbon coating itself is not sufficiently effective at alleviating the interfacial exothermic reaction. It was already reported that a continuous PI coating layer prevents LCO from coming into direct contact with the vigorous liquid electrolyte, thereby mitigating any interfacial exothermic reaction [10–12]. This DSC result demonstrates that the performance of the PI coating layer as an ion-conductive protective nanothin film is not impaired after combination with the electroconductive carbonaceous substance.

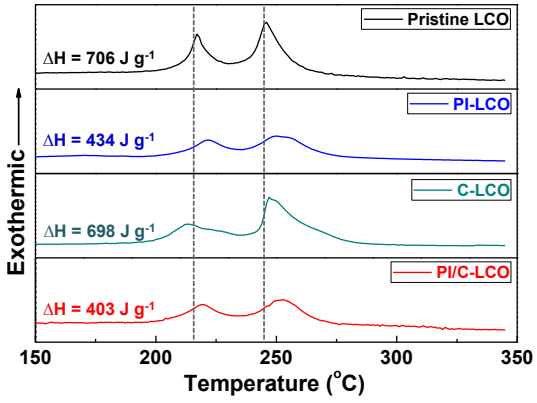

Fig. 6. DSC thermograms showing the interfacial exothermic reaction between delithiated LCO (pristine LCO, C-LCO, PI-LCO, and PI/C-LCO) and liquid electrolyte.

This beneficial effect of the PI/C coating layer on the thermal stability of delithiated LCO is schematically depicted in Fig. 4.

4. Conclusions

As a new concept for engineering surface architecture to address interfacial issues between cathode materials and liquid electrolytes, a mixed ion/electron-conductive protective conformal coating layer based on PI/C soft nanomatter was demonstrated. The in-depth structural characterization of PI/C-LCO confirmed that the PI/C coating layer was successfully synthesized on the LCO surface via one-pot thermal treatment of a polyamic acid and sucrose mixture. A distinctive feature of the PI/C coating layer was that it facilitated electronic conduction while maintaining the beneficial functions as an ion-conductive protective PI nanothin film. This synergistic coating effect improved the high-voltage cell performance and also suppressed the interfacial exothermic reaction between LCO and liquid electrolyte. We envisage that the multifunctional PI/C soft nanomatter-mediated conformal surface modification presented herein holds promise as a facile and versatile way of resolving interfacial problems between electrode materials and liquid electrolytes, thus boosting the development of high-performance lithium-ion batteries with reliable electrochemical/safety attributes.

Acknowledgments

This research was supported by the MKE (The Ministry of Knowledge Economy), Korea, under the ITRC (Information Technology Research Center) support program (NIPA-2012-H0301-12-1009) supervised by the NIPA (National IT Industry Promotion Agency). This work was also supported by the National Research Foundation of Korea Grant funded by the Korean Government (MEST) (NRF-2009-C1AAA001-2009-0093307). This study was supported by the BK21 Plus funded by the Ministry of Education, Korea (10Z20130011057).

Appendix A. Supplementary data

Supplementary data related to this article can be found at http://dx.doi.org/10.1016/j.jpowsour.2014.04.028.

References

[1] M. Armand, J.M. Tarascon, Nature 451 (2008) 652–657.
[2] C. Liu, F. Li, L.P. Ma, H.M. Cheng, Adv. Mater. 22 (2010) E28–E62.
[3] G.J. Jeong, Y.U. Kim, H.S. Kim, Y.J. Kim, H.J. Sohn, Energy Environ. Sci. 4 (2011) 1986–2002.
[4] A. Manthiram, J. Phys. Chem. Lett. 2 (2011) 176–184.
[5] B. Scrosati, J. Hassoun, Y.K. Sun, Energy Environ. Sci. 4 (2011) 3287–3295.
[6] Y. Huang, J. Chen, F. Cheng, W. Wan, W. Liu, H. Zhou, X. Zhang, J. Power Sources 195 (2010) 8267–8274.
[7] S.K. Hu, G.H. Cheng, M.Y. Cheng, B.J. Hwang, R. Santhanam, J. Power Sources 188 (2009) 564–569.
[8] J.P. Cho, Y.W. Kim, B.S. Kim, J.G. Lee, B.W. Park, Angew. Chem. Int. Ed. 42 (2003) 1618–1621.
[9] K.S. Lee, S.T. Myung, D.W. Kim, Y.K. Sun, J. Power Sources 196 (2011) 6974–6977.
[10] J.H. Park, J.S. Kim, E.G. Shim, S.Y. Lee, Electrochem. Commun. 12 (2010) 1099–1102.
[11] J.H. Park, J.H. Cho, S.B. Kim, W.S. Kim, S.Y. Lee, J. Mater. Chem. 22 (2012) 12574–12581.
[12] J.H. Cho, J.H. Park, H.K. Song, S.Y. Lee, Energy Environ. Sci. 5 (2012) 7124–7131.
[13] H. Li, H. Zhou, Chem. Commun. 48 (2012) 1201–1217.
[14] A.E. Javier, S.N. Patel, D.T. Hallinan, V. Srinivasan, N.P. Balsara, Angew. Chem. Int. Ed. 123 (2011) 10022–10025.
[15] K. Wang, R. Cai, T. Yuam, X. Yu, R. Ran, Z. Shao, Electrochim. Acta 54 (2009) 2861–2868.
[16] S.W. Oh, S.T. Myung, S.M. Oh, K.H. Oh, K. Amine, B. Scrosati, Y.K. Sun, Adv. Mater. 22 (2010) 4842–4845.
[17] T. Yang, N. Zhang, Y. Lang, K. Sun, Electrochim. Acta 56 (2011) 4058–4064.
[18] L.Y. Jiang, Y. Wang, T. Chung, X.Y. Qiao, J. Lai, Prog. Polym. Sci. 34 (2009) 1135–1160.
[19] M.C. Choi, Y.K. Kim, C.S. Ha, Prog. Polym. Sci. 33 (2008) 581–630.
[20] K. Kushida, K. Kuriyama, J. Cryst. Growth 237 (2002) 612–615.
[21] R. Kalish, Y. Lifshitz, K. Nugent, S. Prawer, Appl. Phys. Lett. 74 (1999) 2936–2938.
[22] M.J. Matthews, M.A. Pimenta, G. Dressenlhaus, M.S. Dresselhaus, M. Endo, Phys. Rev. B 59 (1999) R6585–R6588.
[23] T. Moon, C. Kim, S.T. Hwang, B. Park, Electrochem. Solid-State Lett. 9 (2006) A408–A411.
[24] B. Lin, Z. Wen, J. Han, X. Wu, Solid State Ionics 179 (2008) 1750–1753.
[25] S.M. Lee, H.S. Kim, T.Y. Seong, J. Alloys Compd. 509 (2011) 3136–3140.
[26] T. Ohzuku, A. Ueda, J. Electrochem. Soc. 11 (1994) 2972–2977.
[27] E.S. Choi, S.Y. Lee, J. Mater. Chem. 21 (2011) 14747–14754.
[28] H.S. Jeong, J.H. Kim, S.Y. Lee, J. Mater. Chem. 20 (2010) 9180–9186.
[29] P. Zhang, L. Zhang, X. Ren, Q. Yuan, J. Liu, Q. Zhang, Synth. Met. 161 (2011) 1092–1097.
[30] S.H. Lee, Y. Cho, H.K. Song, K.T. Lee, J. Cho, Angew. Chem. Int. Ed. 51 (2012) 8748–8752.